NASA-CR-176,982

REPRODUCED COPY

NASA-CR-176982
19860021220

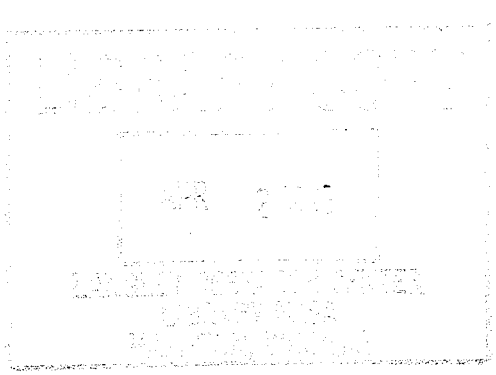

NF01697

AERODYNAMIC DRAG REDUCTION TESTS ON A BOX-SHAPED VEHICLE

FINAL REPORT

PRINCIPAL INVESTIGATORS

Randall Lee Peterson

Doral R. Sandlin

August, 1981

California Polytechnic State University

Aeronautical Engineering Department

San Luis Obispo, California

Grant No. NCC4-1

ACKNOWLEDGEMENTS

The advice and comments of Edwin Saltzman of the Dryden Flight Research Center are gratefully acknowledged. The contributions of many others at DFRC are also acknowledged, especially Ken Illif and Rich Maine of the Dynamics Branch, Jeff Coonrod of the Fabrication and Repair Branch and Vern Wemple of Automotive Maintenence.

The cooperation of several Edwards Air Force Base organizations was also important to the successful completion of this experiment, and their efforts are also gratefully acknowledged. These organizations are: the Base Operations Branch, the Traffic Management Branch and Detachment 21 of the 2nd Weather Squadron (MAC).

I would also like to thank Dr. John D. Nicolaides, my thesis advisor, for the invaluable assistance that he gave on this project. The Dryden Flight Research Center and the California Polytechnic State University, San Luis Obispo participate jointly in a graduate student program funded by NASA under Grant NCC 4-1. The Cal Poly program director is Dr. Doral R. Sandlin. This work was supported by the graduate student grant. I would like to thank both Cal Poly and DFRC for the opportunity to participate in this unique and rewarding program.

TABLE OF CONTENTS

LIST OF SYMBOLS

a	vehicle acceleration
A	body cross-sectional reference area, 3.3 m^2 (35.3 ft^2)
A'	projected cross-sectional reference area used in reference 5 for a 1/10 scale model, based on body plus wheels, at same scale $A' = 1.053\ A$
C_{D_a}	aerodynamic drag coefficient, D_a/qA
D_a	aerodynamic drag
D_e	equivalent diameter, $\sqrt{4A/\pi}$
D_m	mechanical drag
f	rolling resistance coefficient
g	local acceleration due to gravity, 9.795 m/sec^2 (32.137 ft/sec^2)
l	vehicle length
m	vehicle mass, W/g
$\bar{m}$	effective vehicle mass
Δm	additive mass accounting for rotational inertia
p	tire pressure
q	dynamic pressure, $0.5\rho V^2$
R	Reynolds number based on vehicle length, $\rho Vl/\mu$
t	time
V	vehicle velocity
V_o	initial vehicle velocity at $t = 0$

LIST OF SYMBOLS (continued)

W	vehicle weight
μ	absolute viscosity
ρ	air density

LIST OF TABLES

LIST OF FIGURES

INTRODUCTION

Due to the continuing increase in fuel prices and the uncertainty of future supplies, a widespread interest in the efficiency of ground vehicles has developed. Of significant interest are improvements in the aerodynamic efficiency of high volume, "box-shaped" transports, such as delivery vans, motor homes, and trucks. This is because the generally poor aerodynamic shape of these vehicles has so much potential for significant improvement in efficiency.

Prior to the fuel crisis and the rise in fuel prices in 1973 very little was done by the manufacturers of ground vehicles to improve the aerodynamic efficiency. Before that time the high aerodynamic drag of box-shaped transports was overcome by using more powerful engines resulting in increases in fuel consumption. After the fuel crisis numerous drag experiments were conducted on full-scale vehicles and wind tunnel models to improve aerodynamic efficiency.

In 1973 the NASA Dryden Flight Research Center (DFRC) began full-scale tests on a box-shaped van[1]. Various combinations of rounded and square corners were tested. Also tested was a faired and sealed underbody[2]. A 52-percent reduction in drag was obtained by rounding the front corners and a 15-percent reduction in drag was achieved by the

addition of a full-length underbody seal to configuration C of reference 2. Further ground vehicle experimentation at DFRC included add-on drag reduction devices for tractor-trailer combination trucks[3,4].

The present study is a continuation of the tests conducted on the box-shaped vehicle in 1973. The intent of the present experiment is to define a near optimum value of drag coefficient for a high volume type of vehicle through the use of a boattail, on a vehicle already having rounded front corners and an underbody seal, or fairing. The results of these tests will constitute a baseline for later follow-on studies to evaluate candidate methods of obtaining afterbody drag coefficients approaching the boattail values, but without resorting to such impractical afterbody extensions.

The current modifications to the box-shaped vehicle consisted of a full and truncated boattail in conjunction with the faired and sealed underbody. Drag results from these configurations are compared with corresponding wind-tunnel results of a 1/10 scale model.

Test velocities ranged up to 96.6 km/h (60 mph) and the corresponding Reynolds numbers ranged up to 1.3×10^7 based on the vehicles length which includes the boattail. A simple coast-down technique was used to define drag.

TEST VEHICLE

The box-shaped test vehicle used in early ground vehicle studies at NASA-DFRC[1,2] was obtained by modifying an

ordinary commercial cab-over-engine van, figure 1. The various configurations investigated in this study were once again achieved as before by relatively simple changes to the sheet metal and subframe. The dimensions of the original square cornered configuration, as reported in references 1, 2 and 4, are shown in figure 2.

The three configurations investigated in this study were achieved through the addition of a full-boattail and a truncated boattail, configurations II and III respectively, to the baseline box-shaped vehicle, configuration I. Configuration I, which had the same overall length, width and height as the square cornered vehicle shown in figure 2, featured rounded forebody horizontal and vertical corners, a faired and sealed underbody and a blunt aft-end, figure 3. This configuration was used as a baseline, for the present tests, to determine the percent decrease in drag obtained by the addition of the full and truncated boattails. Configuration II consisted of the rounded forebody, the faired and sealed underbody and the full boattail, figure 4. The final configuration, configuration III, consisted of the truncated boattail in conjunction with the same rounded forebody and faired and sealed underbody, figure 5.

The size and contour of the boattail used in this study was determined from somewhat arbitrarily conceived full-scale size limitations, full-scale (DFRC) tuft studies, and wind-tunnel flow visualization studies on a 1/10 scale model (University of Kansas, reference 5). The length of

the boattail from its base to its apex was, for practical considerations, restricted to the width of the test vehicle. This length also approximates the equivalent diameter of the vehicle, D_e. The model flow visualization studies using tufts and neutrally bouyant helium bubbles to trace the streamlines showed that the arbitrarily derived boattail geometry was effective in "closing" the flow to produce a relatively small wake.

The full-scale truncated boattail configuration was a direct result of the model flow visualization studies. The length of the truncated boattail was determined by cutting off the portion of the boattail behind the flow separation station as defined by the model tuft results. Dimensions of the full and truncated boattails are presented in figure 6.

The full-length underbody seal on the test vehicle was configured so that it faired smoothly into the rounded front lower horizontal surface and the bottom quarter of the boattail. An aft facing gap underneath the vehicle permitted the cooling air that passed through the engine radiator to escape during "cooling-vent-open" operation. The aft part of this gap is shown in the lower left portion of figure 7, immediately below the rear portion of the wheel well. Figure 8 shows the full-length underbody seal as viewed from the front.

The front wheel wells were sealed using tape and fiberglass cloth impregnated with silicone rubber to allow

the front suspension system to flex. Figure 7 shows the right front wheel well seal as viewed from a point slightly forward of the right front wheel.

The rear wheel wells were sealed using sheet metal and tape. Vertical slots were provided in the rear wheel seals to allow the rear axle to respond to small road discontinuities without damaging the seals. Figure 9 shows the right rear wheel seal as viewed from a point slightly forward of the rear axle.

EXPERIMENTAL CONCEPT

Newton's second law of motion states that the time rate of change of momentum of a body equals the applied force. In the case of a decelerating vehicle, the applied force is that of aerodynamic and mechanical drag. Thus, since momentum is mass times velocity we have:

$$\frac{d}{dt}\{(\text{mass})(\text{velocity})\} = \text{Force};$$

or

$$\frac{d}{dt}(mv) = F$$

where m = mass, and v = velocity. In the event the mass is constant we conclude;

$$m\frac{dV}{dt} = ma = F$$

for the case of a road vehicle decelerating from a high speed, the total drag equals the mass times the deceleration.

The following equation results for a road vehicle decelerating from a high speed.

$$\bar{m}a = -0.5\rho V^2 C_{D_a} A - fW \qquad (1)$$

The term on the left-hand side of the equation is the effective mass times the acceleration. The first term on the right-hand side is the aerodynamic drag force, and the second term is the mechanical drag force.

The aerodynamic drag force is assumed to be a function of velocity squared, where the aerodynamic drag coefficient (C_{D_a}) is virtually independent of velocity. The mechanical drag consists of the tractive drag of the tires, bearings and seals, the gear resistance of the differential and drive train and the thrust due to the rotational inertia of the wheels and tires.

Because the mechanical drag was essentially independent of configuration and because of the large number of variables involved, an analytical description of the mechanical drag is considered to be outside the scope of this study. Therefore, the variation of tractive drag with velocity, with the tires being the major source, was approximated using Hoerner's equation for rolling resistance[6]. The variation of the tractive drag with velocity as approximated by Hoerner's equation for rolling resistance was extrapolated from a nearly "static" level measured value of tractive drag. Hoerner's equation for rolling resistance coefficient is:

$$f = 0.005 + (0.15/"p") + (0.000035\ V^2/"p") \qquad (2)$$

where p = tire pressure (psi), and V = velocity (mph).

Hoerner's rolling resistance is approximately proportional to the load under which the wheels are moving. The rolling resistance coefficient is primarily dependent upon the inflation pressure "p", and to a minor extent upon the velocity of the vehicle. The rolling resistance of the tires is not independent of velocity and to assume such can cause major errors in the determination of aerodynamic drag from coast-down tests.

The second part of the mechanical "drag" is due to the rotational kinetic energy of the tires and wheels. The thrust due to the rotational inertia of the tires and wheels is taken into account in the correction of the vehicle's mass. The effective mass of the vehicle is then $\bar{m}$, where $\bar{m} = m + \Delta m$ and Δm is the correction for rotational inertia. For this analysis the Δm value used to account for the rotational inertia, as determined from torsional pendulum tests of the tires and wheels, is 2.4-percent of the vehicle's mass or $\bar{m} = 1.024$ times the actual mass, m.

DATA REDUCTION

In this analysis of coast-down data, an analytical model was used to separate the mechanical drag from the aerodynamic drag. Because of the nature of the data obtained from the coast-down tests, a relationship expressing velocity

as a function of time was needed to determine the aerodynamic drag contribution of the total drag. To obtain this relationship, equation 1 was integrated with respect to time after the inclusion of Hoerner's semiempirical equation for rolling resistance. The result of this integration is:

$$V(t) = (B/\sqrt{BA}) \tan(\tan^{-1} Vo(\sqrt{BA}/B) - \sqrt{BA}(t)) \qquad (3)$$

where; $A = (0.5\rho C_{D_a} A)/\bar{m} + 0.000035(W/\bar{m}p)$

$B = 0.005 + (0.15/p)$

(see appendix A for the complete integration process).

To analyze the coast-down data a computer program was written to determine the aerodynamic drag and the aerodynamic drag coefficients. This program (VEHICLE) utilized a subroutine (ZXSSQ) from the International Math and Statistics Library. The subroutine ZXSSQ solves nonlinear least squares problems using a modified finite difference, Levenberg-Marquardt algorithm. This modification eliminates the need for explicit derivatives. The purpose of ZXSSQ was to find the minimum of the sum of squares of M functions in N variables using the velocity-time data obtained from the coast-down tests as residuals in equation 3. See appendix B for a listing of the program VEHICLE.

In this analysis, the mechanical (tractive) drag was extrapolated from an experimentally measured value obtained at very low velocities, where the aerodynamic drag and the inertial thrust effects could be neglected. The aerodynamic drag on the other hand was an unknown and

therefore the aerodynamic drag coefficient (C_{D_a}) was written into equation 3 and the computer program as a variable, X(1). From the input residuals (velocity-time data), the aerodynamic drag coefficients and the aerodynamic drag at the corresponding velocity intervals were determined. Methods of analyzing coast-down data which have been used by other investigators are presented in references 7 to 10.

COAST-DOWN METHOD

Coast-down tests are used to experimentally determine the rolling resistance and the aerodynamic drag of road vehicles. This technique has been demonstrated to be a practical method for obtaining high quality drag data for road vehicles under a simulation of actual operating conditions, provided that sufficient care is taken in the details of the test technique. This technique is attractive because of its simplicity and low cost. It also permits data to be obtained at any desired velocity range and in both directions on the test surface.

The coast-down technique consists of accelerating the vehicle to a few miles-per-hour above the starting velocity of each test whereupon the manual transmission is disengaged to allow the vehicle to decelerate in neutral. The time it takes for the vehicle to slow to given velocities is then recorded and used to calculate the vehicle drag. The vehicle was weighed, with occupants, before and after each series of tests to provide the proper mass for computing

drag (a "series of tests" is meant herein to refer to the test runs accomplished during a given day).

The mechanical drag of the test vehicle was measured experimentally at very low velocities after each series of tests. This was done by slowly towing the vehicle over a level surface using a hand held spring scale. The measured force was then used as an endpoint in the extrapolation of Hoerner's rolling resistance equation. This extrapolation was assumed to account for the entire mechanical resistance of the test vehicle while decelerating in neutral. The vehicle began each day of testing with a tire pressure of 2.48×10^5 pascals (36 lb/in^2). Figure 10 shows the final approximation of mechanical drag as a function of velocity.

All of the drag data for the box-shaped vehicle were obtained during cooling-vent-closed operation. This was done so that the effect of the cooling drag could be eliminated during each coast-down run. The cooling vent was opened between runs and during vehicle acceleration so that overheating of the engine would not occur. A portion of the cooling vent door may be seen at the extreme front of the vehicle in figure 5 whereas, in contrast, the vent was closed in figure 3.

The final drag results for the full and truncated boattail configurations were obtained by subtracting the incremental drag of the fifth-wheel and the fifth-wheel support system (figure 11) from the measured overall drag values containing the "side-mounting" drag increment. The

blunt aft-end, baseline configuration was used to determine this increment as it had a fifth-wheel mount located on the blunt aft-end of the vehicle (figure 12), which was not usable in the full and truncated boattail configurations. The incremental drag of the "side-mounted" fifth-wheel and support system was determined by subtracting the coast-down results obtained with the trailing fifth-wheel, on configuration I, from the "side-mounted" coast-down results, also obtained from configuration I. Figure 13 shows these data over the range of test velocities.

All of the drag data for the box-shaped vehicle were obtained using the coast-down technique. The deceleration of the vehicle was measured using a bank of five 0.1-second stopwatches and a calibrated, fifth-wheel driven, precision speedometer which provided a 0.1-mile per hour readout capability.

INSTRUMENTATION

A fifth-wheel was used in this study to accurately measure the velocity of the box-shaped test vehicle. In use, the fifth-wheel trails the test vehicle and continues to rotate, or measure speed and/or distance, while the vehicle is in motion.

The fifth-wheel system transmits miles-per-hour and/or trip mileage by cables to digital readout speedometer and odometer units located inside the test vehicle. The fifth-wheel system operates by sending pulse counts based

on the rotation of the wheel to these instrument units. The instruments operate from a 12-volt negative ground battery system which can either be the vehicle's battery or a secondary battery. When properly calibrated, a fifth-wheel will accurately measure velocity and/or distance.

Calibration of the fifth-wheel is achieved by varying the tire pressure. Reducing the tire pressure increases the indicated speed and distance and increasing the pressure will reduce the indicated speed and distance. When properly calibrated, the system accuracy is within 0.1-percent of the total distance (maximum variation of 5 feet in one mile). Calibration of distance automatically calibrates the velocity due to the crystal controlled clock. The crystal controlled clock is accurate within 0.02-percent, thus providing accurate measurements of velocity. Speed readouts are within $\pm$ 0.5 mph of the true vehicle speed at speeds from 0 to 150 mph.

The calibration of the fifth-wheel was accomplished on the auxiliary runway used in the coast-down tests. An accurately laid out distance course was measured for calibration purposes. The calibration of the fifth-wheel was completed using a trial and error method. The fifth-wheel tire pressure was varied depending on the distance measurement at the end of each calibration run. The resulting cold tire pressure was 36 psi. The fifth-wheel distance calibration was periodically checked after coast-down runs and was determined to be within $\pm$ 0.05-percent of the actual

distance (maximum variation of 1 foot in 2000 feet).

The time increments corresponding to preselected velocity intervals were measured using a bank of five 0.1-second stopwatches. The time increments corresponding to preselected velocity intervals in miles-per-hour (i.e., 60 to 55, 55 to 50, 50 to 45, 45 to 40, and 40 to 35) were obtained by starting all the stopwatches simultaneously at the starting velocity and stopping them individually at the end of each preselected velocity interval. The stopwatch data were then hand recorded at the end of each test run. Figure 14 shows the layout of the instrumentation in the vehicle.

TEST CONDITIONS

All of the coast-down tests were made on an auxiliary runway at Edwards Air Force Base, CA. This runway had an exceptionally smooth asphalt surface and a constant elevation gradient of 0.08-percent. The gradient effects on the deceleration were small and were essentially eliminated by the averaging of successive runs in opposite directions. The averaging of successive runs in opposite directions also accounted for head or tail wind effects provided wind conditions remained constant over the duration of both runs. It should be emphasized, however, that test runs were made early in the day when it was quite calm which virtually eliminated wind effects on the vast majority of test runs.

Wind velocity and direction, ambient pressure and

temperature were recorded every 15 minutes at the Edwards Air Force Base weather station during each day's series of tests so that the air density could be calculated and general atmospheric factors could be taken into account. The test vehicle was driven to and from the auxiliary runway, a distance of approximately 15.3 kilometers (9.5 miles). This provided a pretest warm-up which also brought the temperature of the oil in the differential up to an essentially steady-state level, thus minimizing the variation of this effect from test-run to test-run.

RESULTS AND DISCUSSION

Flow Visualization

Tuft patterns for the full boattail configuration (configuration II) at a speed of 116.7 km/h (72.5 mph) are shown in figures 15 and 16. Both figures show that the flow separates at or just slightly aft of the horizontal and vertical tape lines nearest the apex of the boattail. Figure 15 clearly shows that the flow remains attached over the bottom quarter of the boattail up to this tape line. The achievement of attached flow over the bottom surface of the boattail was considered to be an important factor relative to the overall objectives of this experiment, i.e., determining a near optimum level of drag for a high volume transport type of vehicle through the use of a boattail.

Tuft patterns for the truncated boattail

configuration (configuration III) at a speed of 107.8 km/h (67 mph) are shown in figures 17 and 18. Figure 17 clearly shows the attached flow over the top, the bottom and the left side of the truncated boattail. The dangling white tufts in figure 17 show the stagnant conditions that one would expect on a blunt base moving perpendicular to the airflow. Figure 18 shows a more comprehensive view of the attached airflow over the wetted surfaces of the vehicle and the stagnant conditions over the base of the truncated boattail.

Aerodynamic Drag

The aerodynamic drag is presented in figure 19 for each configuration as a function of velocity. The curve for each configuration is a fairing of the coast-down results using a least squares polynomial regression analysis. The curves for all three configurations are presented for comparison purposes on the composite plot in figure 20.

Aerodynamic drag coefficients for each configuration as obtained from the present full-scale tests (DFRC) and corresponding wind-tunnel tests (KU) are summarized in Table I. The full-scale configuration results are for vehicle speeds of 96.6 km/h (60 mph) and 80.5 km/h (50 mph), which for the purposes of this report are considered to be "highway speeds." All of these data are for the cooling vent closed condition so that a more meaningful comparison can be made with the wind-tunnel model results.

The percentage reduction in drag coefficient for both the full-scale tests and the corresponding wind-tunnel tests was obtained by dividing the incremental drag coefficient by the appropriate baseline value. The percentage difference between the wind-tunnel drag coefficient and the full-scale average drag coefficient for each configuration was obtained by dividing their difference by the full-scale average value.

The results given in the table indicate that an average 32-percent reduction in aerodynamic drag was attained with the addition of the full boattail to the blunt aft-end, baseline configuration at vehicle speeds from 80.5 km/h (50 mph) to 96.6 km/h (60 mph), i.e., highway speeds. The corresponding wind-tunnel results indicated that a 37-percent reduction in aerodynamic drag was attained on the 1/10 scale model at a Reynolds number of 2.7×10^6. The table also indicates that an average reduction of 31-percent in aerodynamic drag was attained with the truncated boattail on the full-scale vehicle over the same range of highway speeds while corresponding wind-tunnel results showed a 38-percent reduction in aerodynamic drag. The incremental drag coefficient of the side-mounted fifth-wheel and the fifth-wheel support system was determined to be 0.030 ($\Delta C_{D_a} = 0.030$) at a vehicle speed of 96.6 km/h (60 mph).

The relatively small difference between configurations II and III (for V = 96.6 km/h (60 mph)) indicates that the boattail was cut in approximately the right place. This small

drag increment, approximately 3.8-percent at this velocity, shows that it is possible to eliminate the additional length and ineffectual volume of the boattail apex while retaining almost all of the aerodynamic effectiveness of the complete boattail. At a speed of 80.5 km/h (50 mph) or lower, the drag coefficients of configurations II and III are essentially the same, thus establishing the truncated boattail as, overall, the most efficient of the two on the basis of aerodynamic drag and useful volume.

The drag reductions provided by the boattails in the present experiment and in reference 5 are very significant, but they should be interpreted with caution. As was mentioned on page 14, "the achievement of attached flow over the bottom surface of the boattail was considered to be an important factor relative to the overall objectives of this experiment, i.e., determining a near optimum level of drag for a high volume transport type vehicle through the use of a boattail." That is to say, it is necessary to provide attached flow upstream of all boattail surfaces in order to maximize the reduction in afterbody drag. Thus, the rounded forebody corners and the smooth, sealed underbody of the baseline vehicle, configuration I, provided a near ideal candidate vehicle for demonstrating good boattail performance. The reader is hereby forewarned that the addition of a boattail to a configuration having separated flow, or perhaps even relatively low energy flow, over one or more upstream surfaces may result in significantly smaller drag reductions

than demonstrated herein or in reference 5 (see references 11 and 12 for examples).

It is also interesting to note that although the aerodynamic drag coefficient (C_{D_a}) was assumed to be constant with velocity in this analysis, in actuality it was found to vary with vehicle velocity. The variation of aerodynamic drag coefficient with vehicle velocity for all configurations is shown in figure 21. This figure shows that the aerodynamic drag coefficient decreases with increasing vehicle velocity. This decrease is due to the higher energy of the flow and the delay in separation over the aft-end of the vehicle.

CONCLUDING REMARKS

The effectiveness of the full boattail in delaying flow separation over the aft-end of the vehicle (reducing the size of the wake) is apparent in the average 32-percent reduction in aerodynamic drag as compared to the baseline drag at highway speeds. The relative effectiveness of the truncated boattail is similarly apparent in the average 31-percent reduction in aerodynamic drag as compared to the baseline configuration.

The small drag increase, approximately 3.8-percent at 96.6 km/h (60 mph), which occurred when the boattail was truncated indicates that the boattail was cut in approximately the right place. This relatively small increase in

drag shows that it is possible to eliminate the additional length and ineffectual volume of the boattail apex while retaining almost all of the aerodynamic effectiveness of the full boattail. The drag coefficients of the full and truncated boattails are essentially the same for speeds of 80.5 km/h (50 mph) and lower. Thus the truncated boattail is the more efficient of the two, overall, on the basis of aerodynamic drag and useful volume.

The aerodynamic drag coefficients and the percentage reduction in drag obtained by the addition of the full and truncated boattails to the baseline configuration in this study were obtained using an approximation for rolling resistance. However, it is felt that future work in the area of coast-down analysis should be conducted where both the aerodynamic drag coefficient (C_{D_a}) and the rolling resistance coefficient (f) are treated as variables. This will provide a greater accuracy in the determination of precise values of C_{D_a} for a specific configuration.

REFERENCES

1. Saltzman, E. J. and Meyer, R. R., Jr., "Drag Reduction Obtained by Rounding Vertical Corners on a Box-Shaped Ground Vehicle," NASA TM X-56023, March 1974.

2. Saltzman, E. J., Meyer, R. R., Jr., and Lux, D. P., "Drag Reductions Obtained by Modifying a Box-Shaped Ground Vehicle," NASA TM X-56027, October 1974.

3. Montoya, L. C. and Steers, L. L., "Aerodynamic Drag Reduction Tests on a Full-Scale Tractor-Trailer Combination with Several Add-On Devices," NASA TM X-56028, December 1974.

4. Steers, L. L., Montoya, L. C., and Saltzman, E. J., "Aerodynamic Drag Reduction Tests on a Full-Scale Tractor-Trailer Combination and a Representative Box-Shaped Ground Vehicle," Society of Automotive Engineers, Paper SAE 750703, August 1975.

5. Muirhead, V. U., "An Investigation Of Drag Reduction On Box-Shaped Ground Vehicles," KU-FRL #180, July 1976, The University of Kansas.

6. Hoerner, S. F., "Fluid-Dynamic Drag," published by the author (148 Busteed Dr., Midland Park, N. J.), 1965.

7. White, R. A. and Korst, H. H., "The Determination of Vehicle Drag Contributions from Coast-Down Tests," Society of Automotive Engineers, Paper SAE 720099, January 1972.

8. Korst, H. H. and White, R. A., "Evaluation of Vehicle Drag Parameters From Coast-Down Experiments Conducted Under Non-Ideal Enviromental Conditions," Presented at Joint ASME-CSME Applied Mechanics Fluids Engineering and BioEngineering Conference - Niagara Falls, New York, June 18-20, 1979.

9. Dayman, B., Jr., "Effects of Realistic Tire Rolling Resistance upon the Determination of Aerodynamic Drag from Road-Vehicle Coast-Down Tests," Proceedings of the Second AIAA Symposium on Aerodynamics of Sports and Competition Automobiles, Vol. 16, Western Periodicals, Los Angeles, CA. 1975, pp. 229-238.

10. Dayman, B. Jr., "Tire Rolling Resistance Measurements from Coast-Down Tests," Society of Automotive Engineers, Paper SAE 760153, February 1976.

11. Muirhead, V. U., "An Investigation of Drag Reduction for Tractor Trailer Vehicles with Air Deflector and Boattail," NASA CR-163104, January 1981.

12. Muirhead, V. U., "An Investigation of Drag Reduction for a Standard Truck with Various Modifications," NASA CR-163107, May 1981.

FIGURES AND TABLES

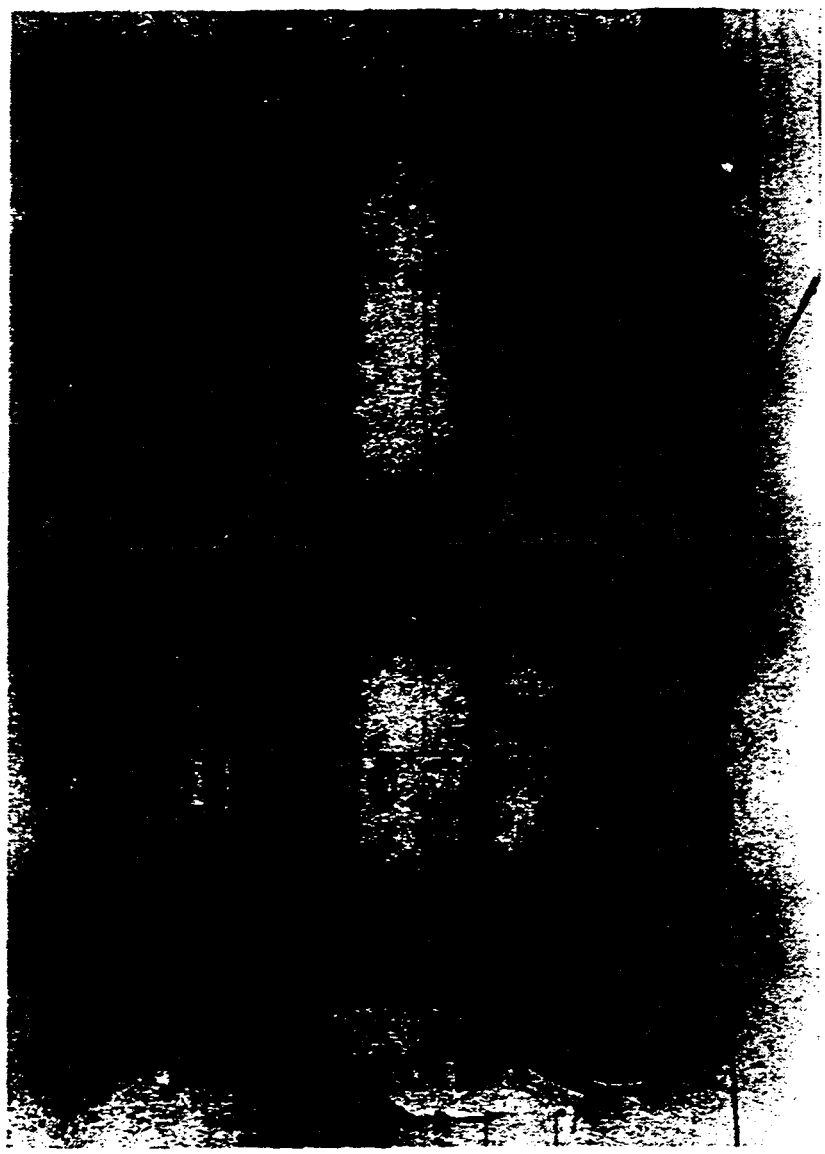

E-26452

Figure 1. Carrier vehicle

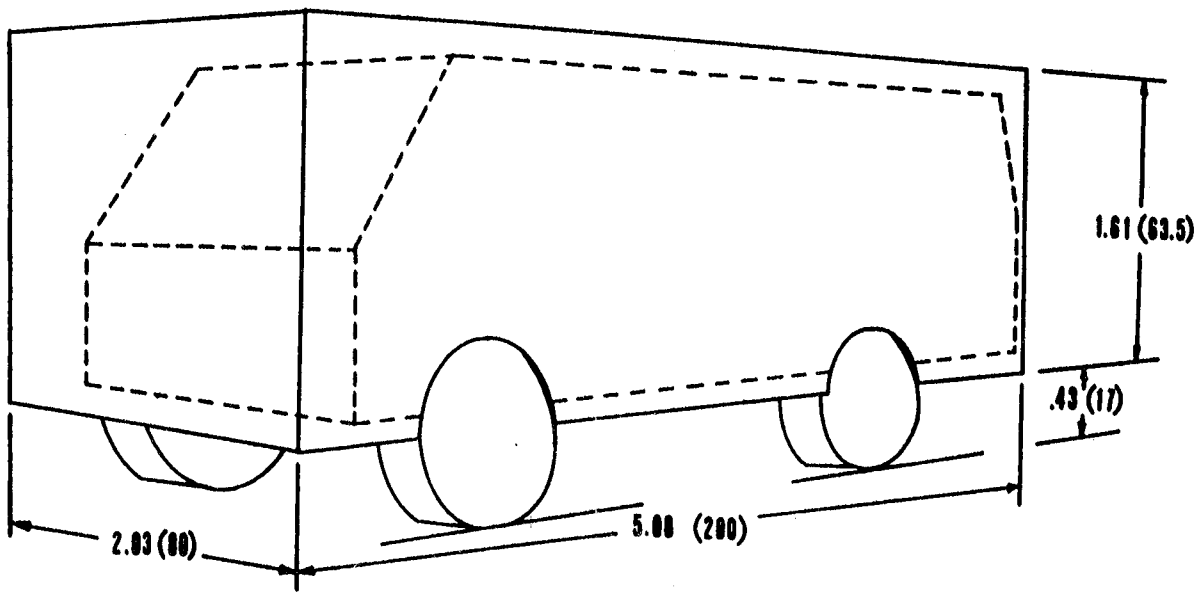

Figure 2. Dimensions of original square-cornered configuration in meters (inches), reference 1.

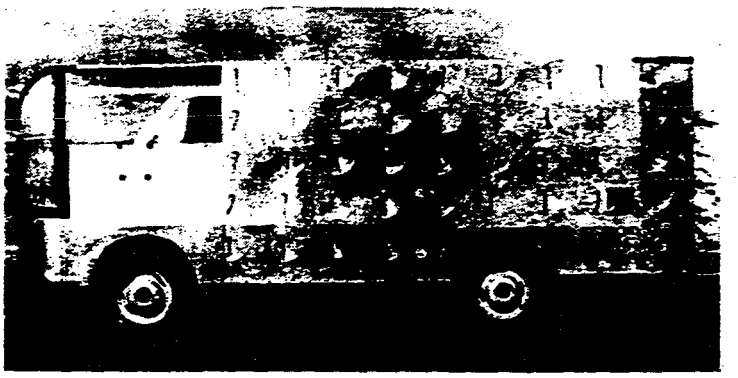

E-38163

Figure 3. Configuration I, V = 0 (engine cooling door closed).

E-38011

Figure 4. Configuration II, vehicle in motion.

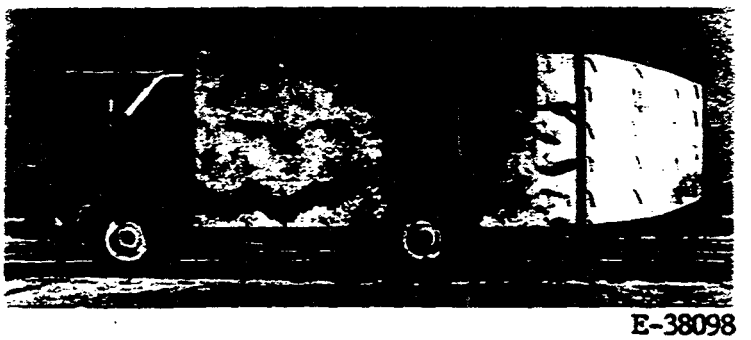

E-38098

Figure 5. Configuration III, V = 0 (engine cooling door open).

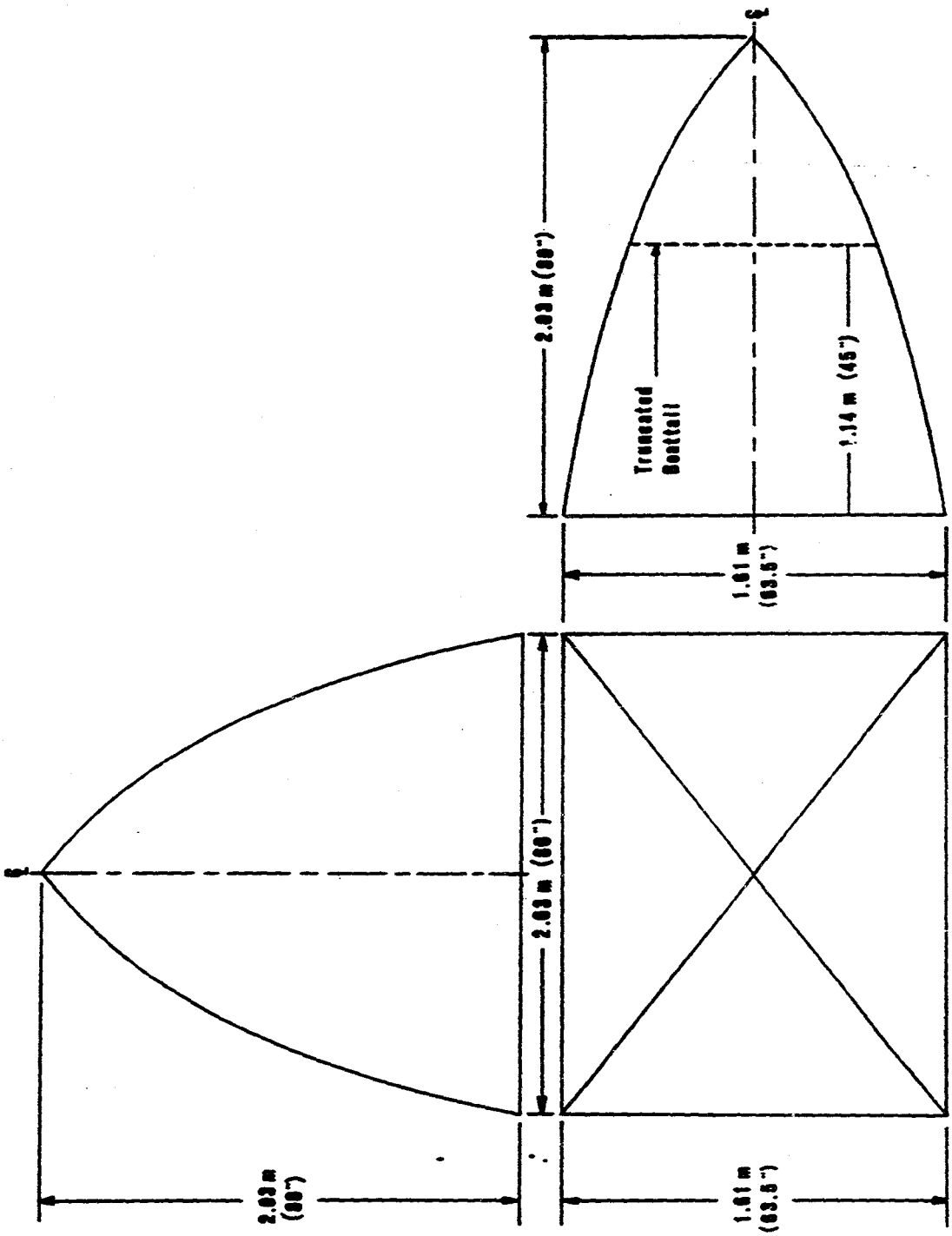

Figure 6. Boattail Dimensions.

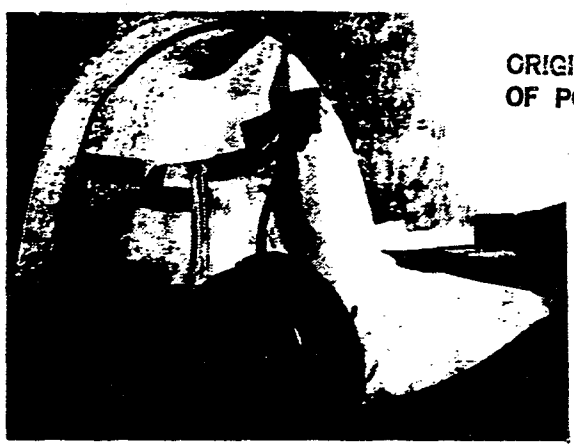

E-37851

Figure 7. **Right front wheel well seal as viewed from slightly ahead of wheel station.**

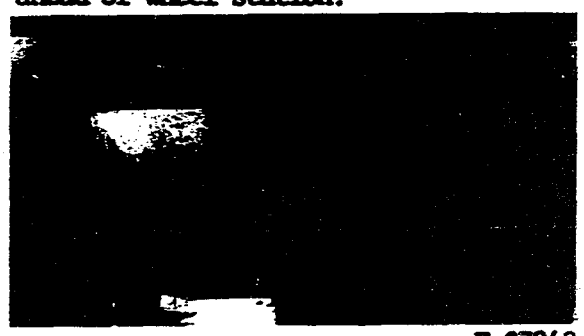

E-37848

Figure 8. **Sealed underbody as viewed from the front.**

E-37854

Figure 9. Right rear wheel well seal as viewed from slightly ahead of axle.

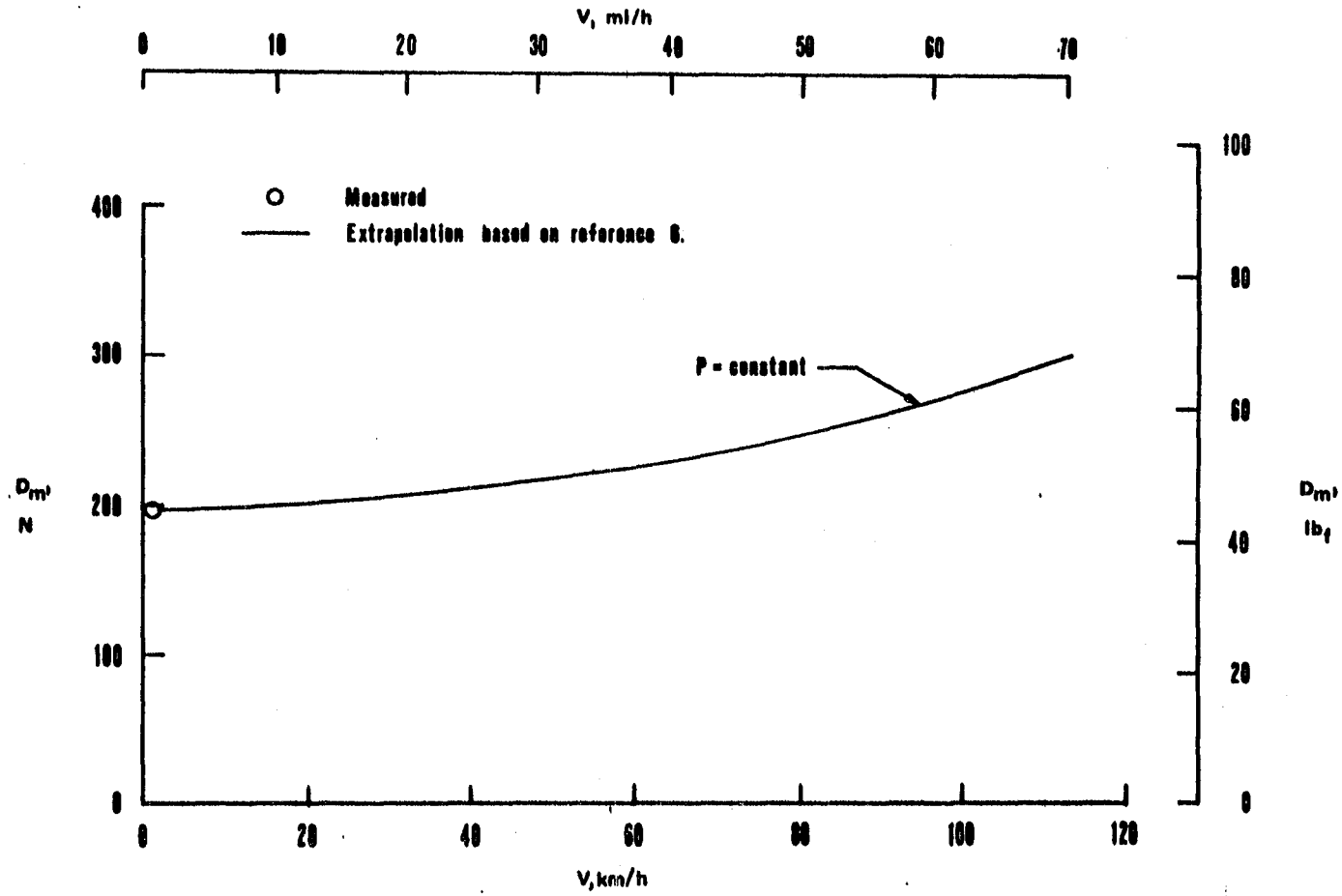

Figure 10. Variation of mechanical drag with vehicle velocity.

E-38161

Figure 11. Fifth-wheel and fifth-wheel support system, "side mounting" (configuration I).

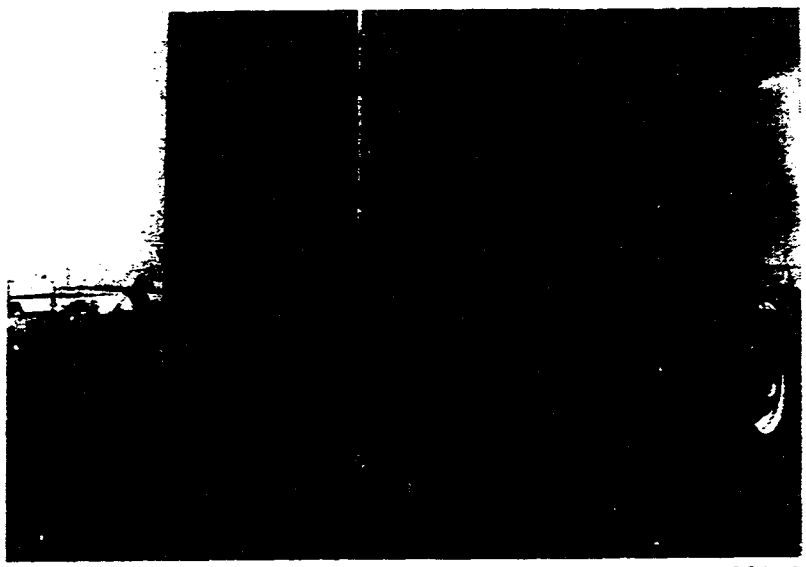

E-38158

Figure 12. Fifth-wheel in aft mounting or trailing location (configuration I).

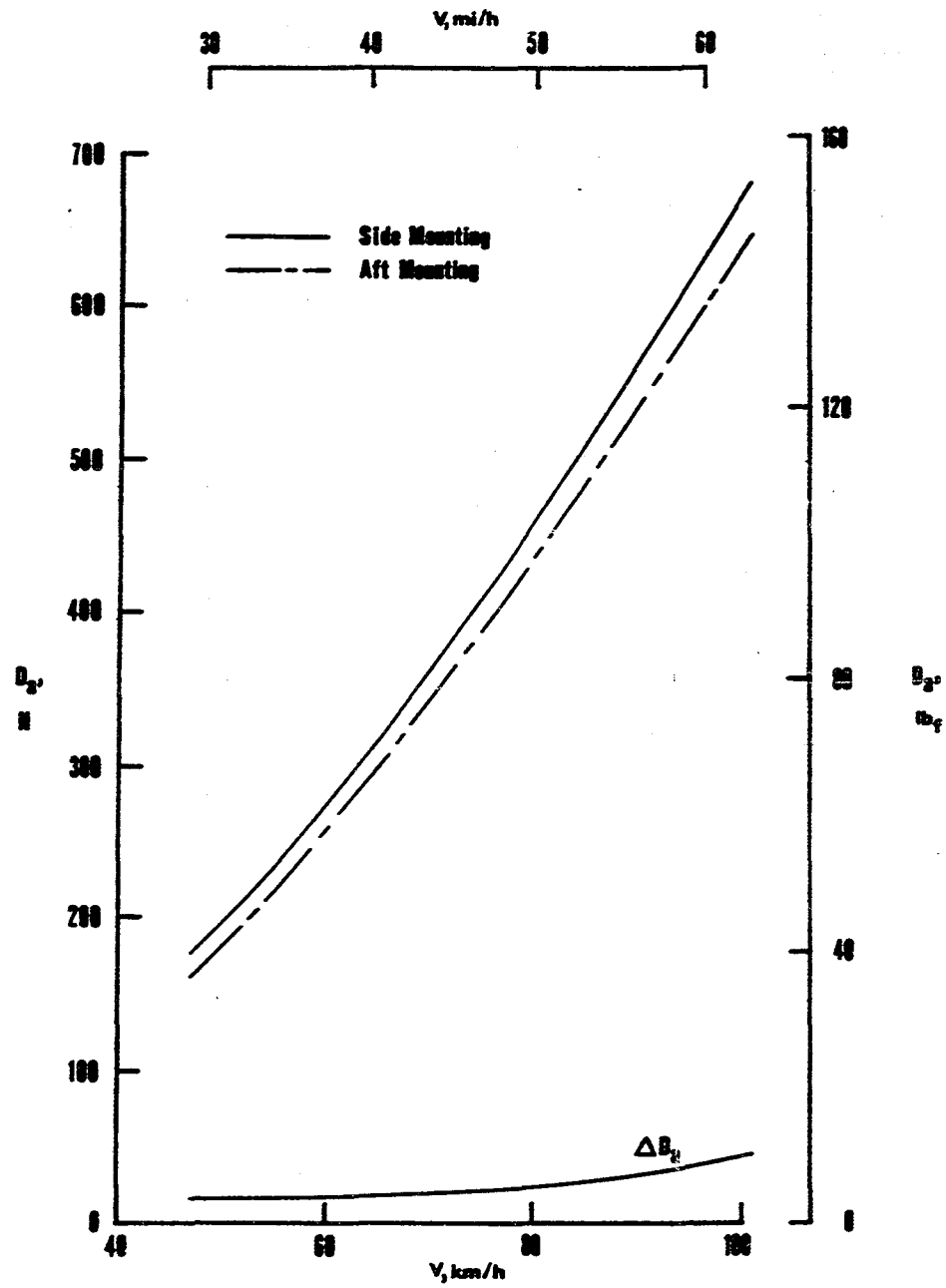

Figure 13. Variation of aerodynamic drag with vehicle velocity for the different fifth-wheel mounting locations, (Configuration I).

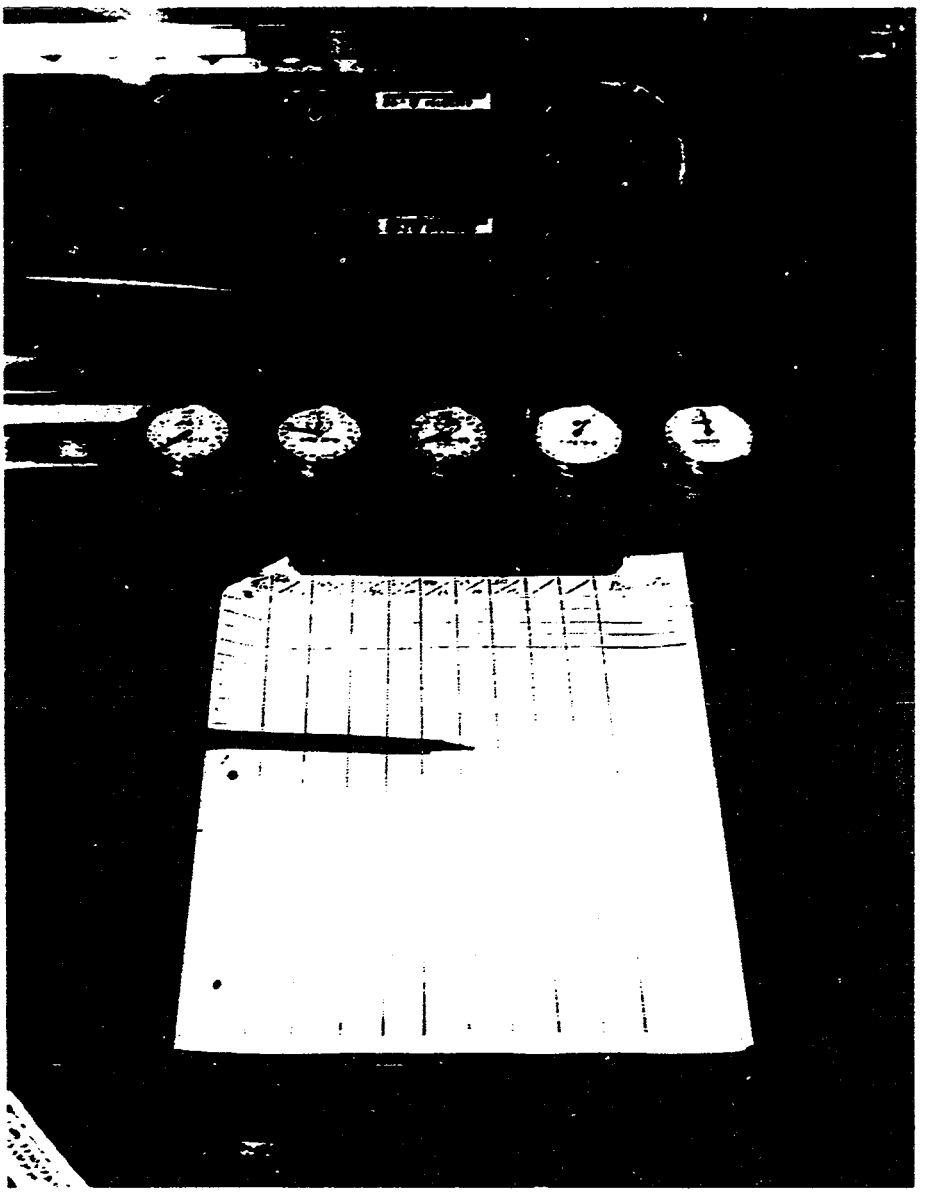

E-38164

Figure 14. Instrumentation layout.

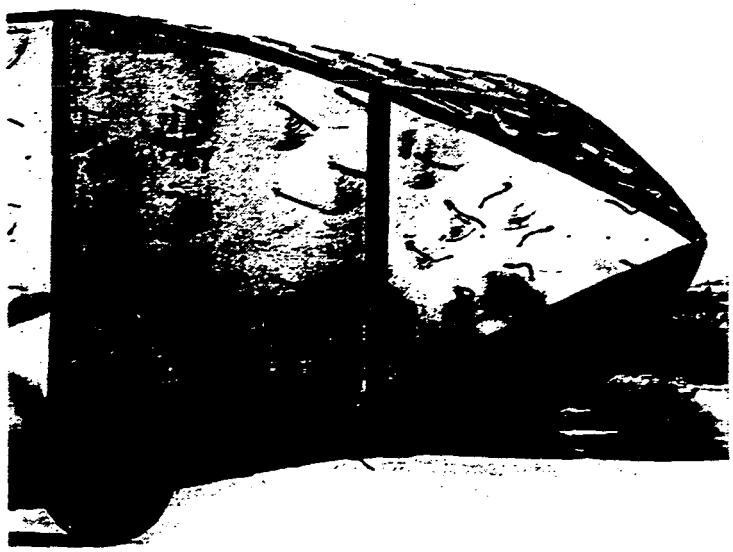

E-38010

Figure 15. Tuft patterns for full boattail, configuration II. V = 116.7 km/h (72.5 mph).

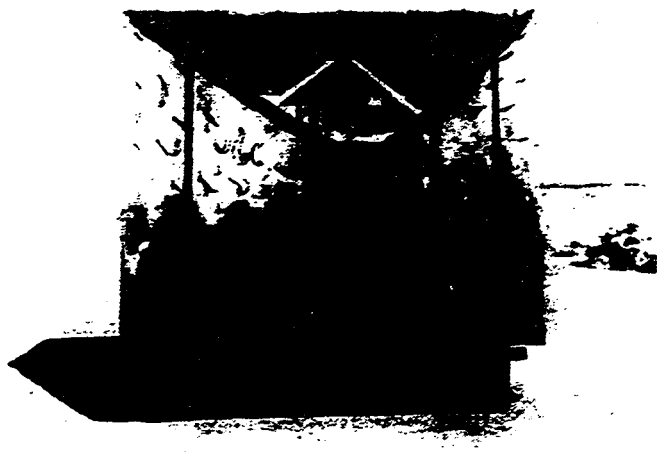

E-38008

Figure 16. Tuft patterns for full boattail, configuration II, V = 116.7 km/h (72.5 mph).

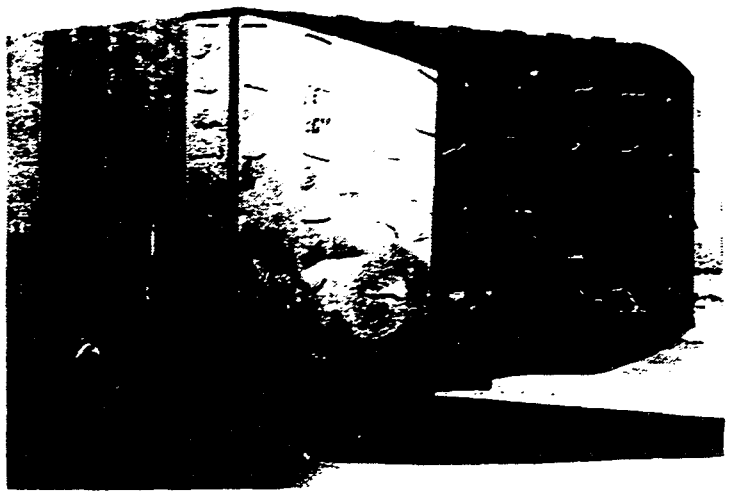

E-38073

Figure 17. Tuft patterns for truncated boattail, configuration III, V = 107.8 km/h (67 mph) (note "dangling" white tufts over base region).

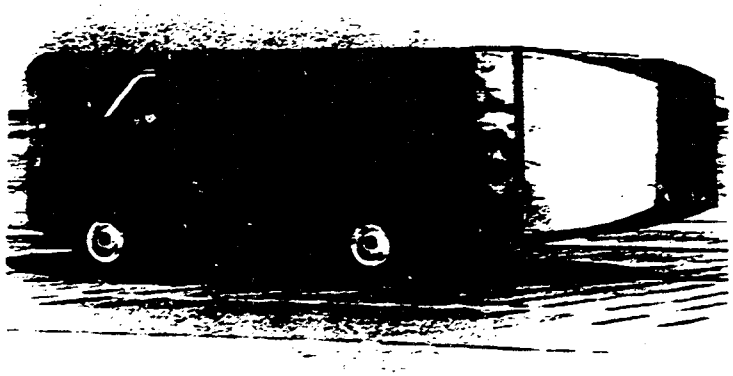

E-38091

Figure 18. Tuft patterns for truncated boattail, configuration III, V = 107.8 km/h (67 mph) (note "dangling" white tufts over base region).

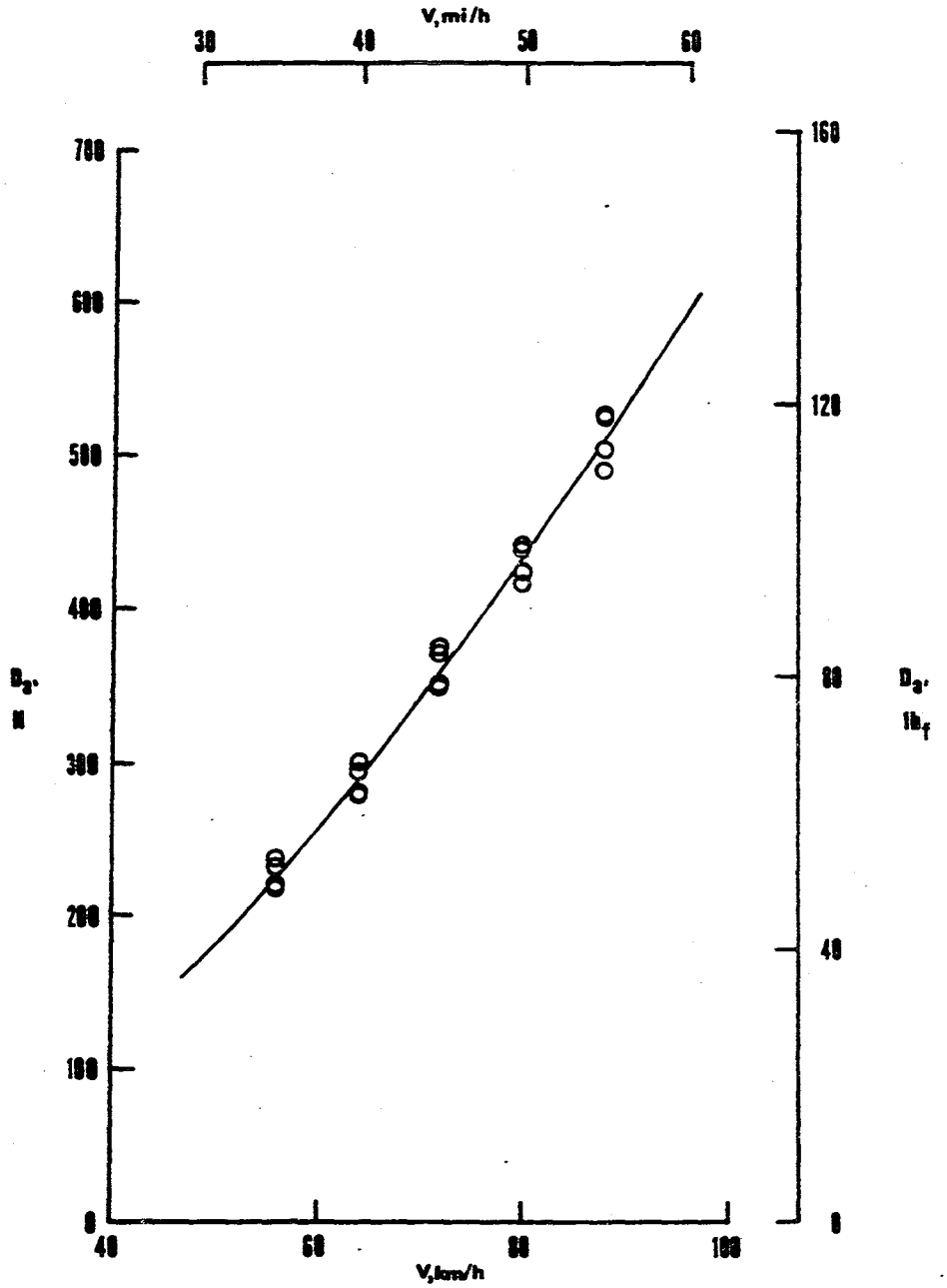

(a) Configuration I, blunt base.

Figure 19. Variation of aerodynamic drag with vehicle velocity, drag increment of side mounted fifth-wheel and support system has been removed,(ΔD_a of figure 13).

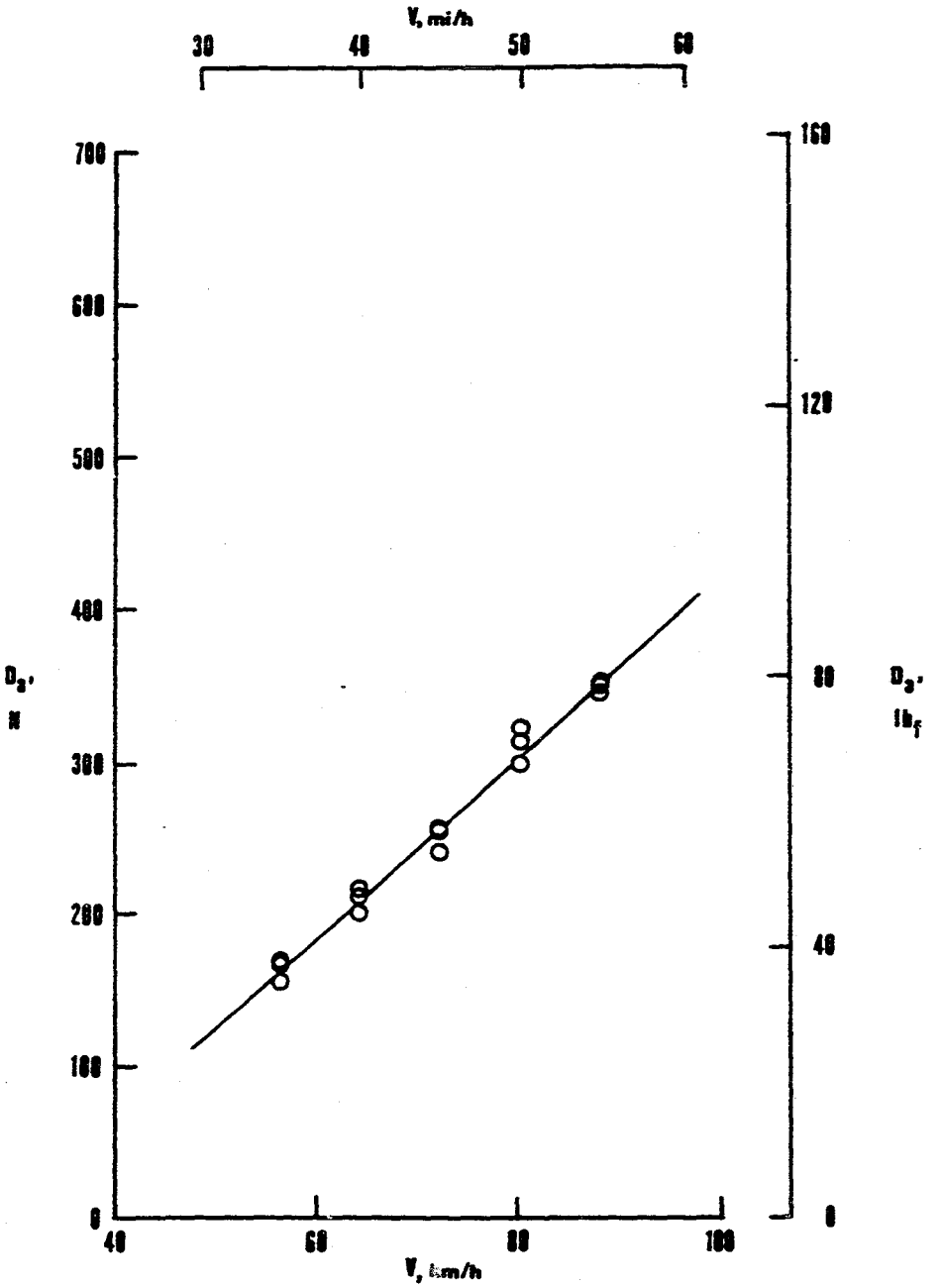

(b) Configuration II, full boattail.

Figure 19. Continued.

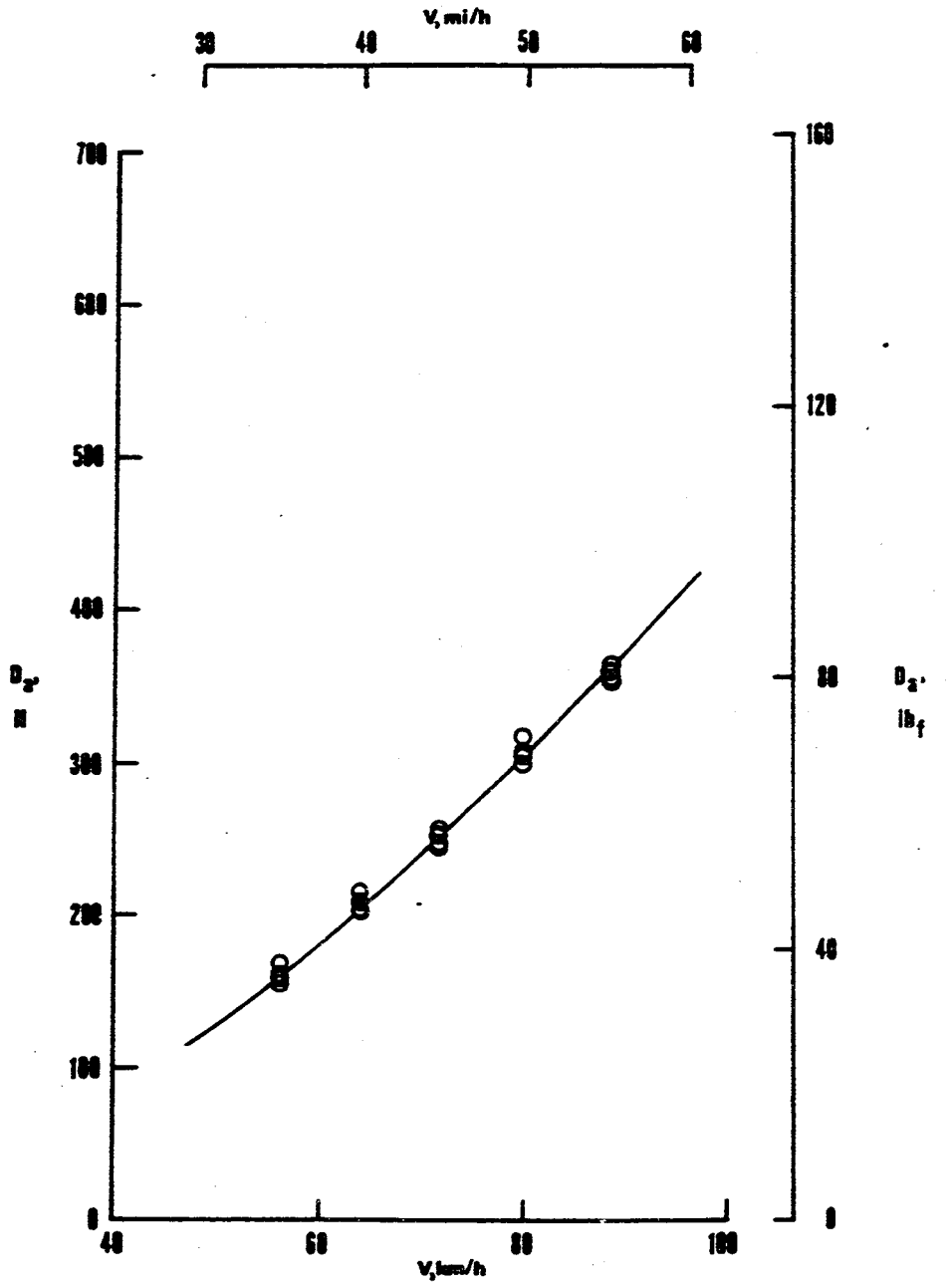

(c) Configuration III, truncated boattail.

Figure 19. Concluded.

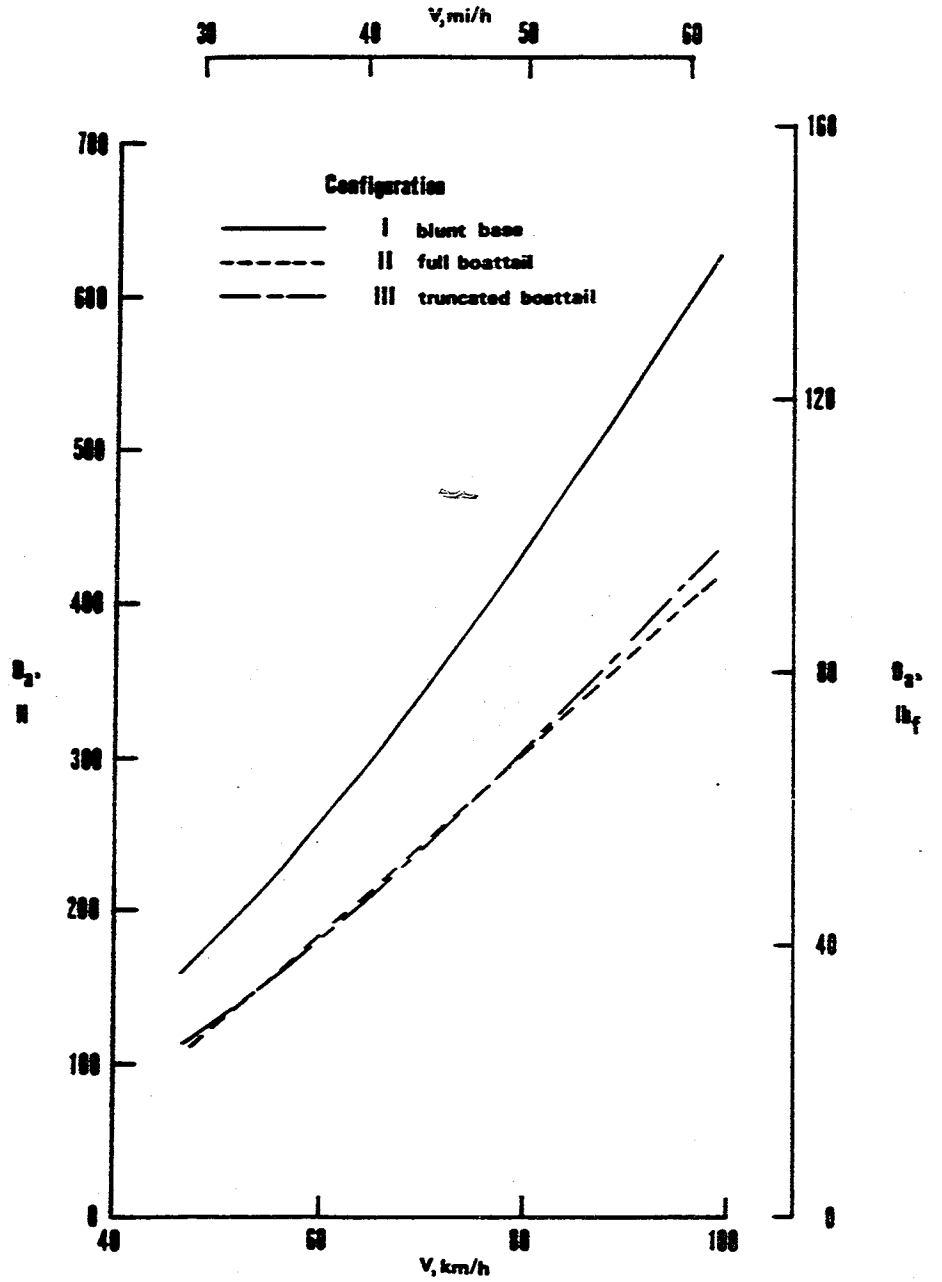

Figure 20. Aerodynamic drag variation with vehicle velocity for all configurations, same data as shown in figure 19.

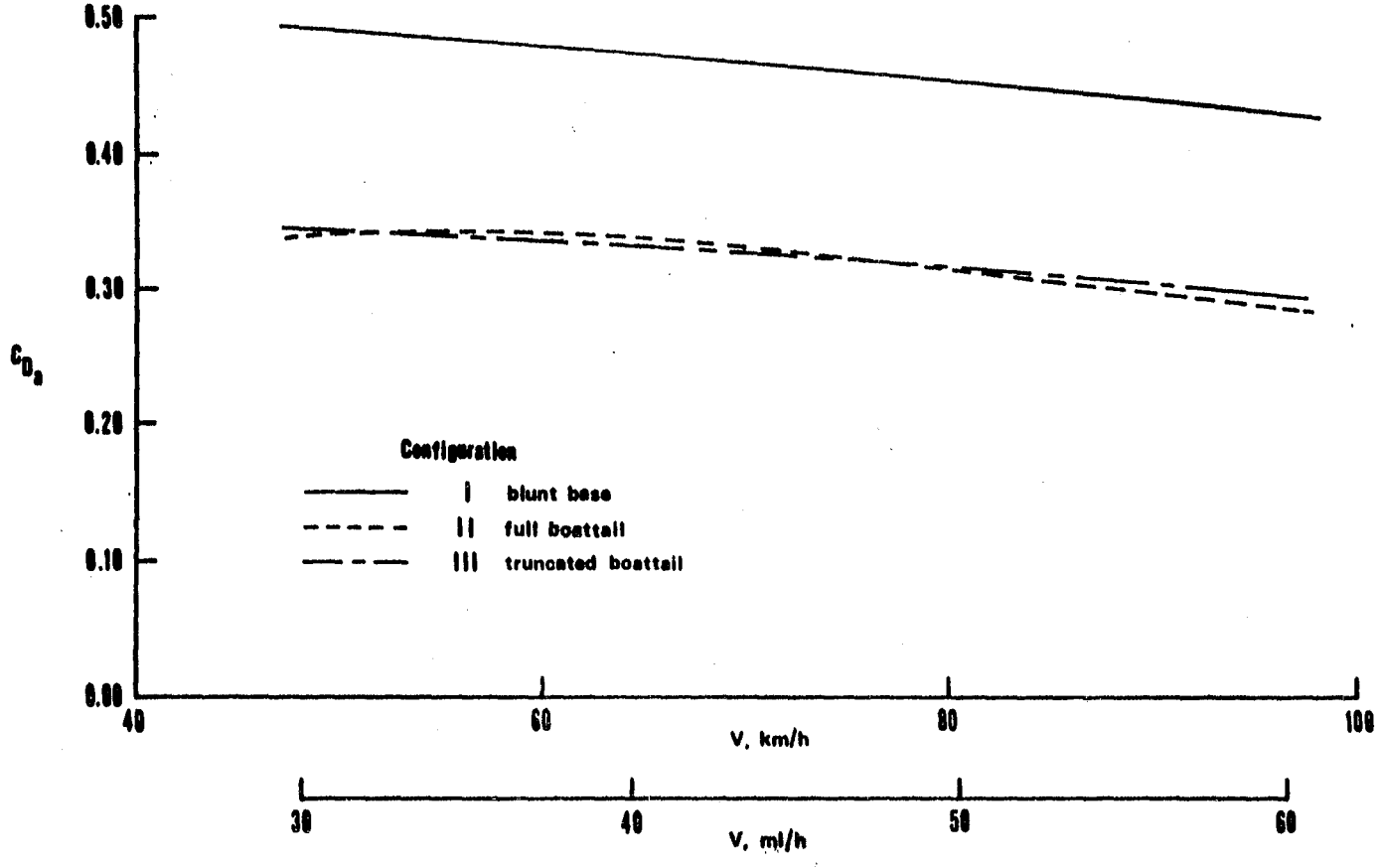

Figure 21. Aerodynamic drag coefficient variation with vehicle velocity for all configurations.

Table I. Comparison of tests run at the Dryden Flight Research Center and the University of Kansas.

Configuration		C_{D_a}, DFRC $R = 1.3 \times 10^7$			C_{D_a}, KU $R = 2.7 \times 10^6$	C_{D_a}, reduction, percent		C_{D_a} - C_{D_a} DFRC,avg. KU / C_{D_a} DFRC,avg. percent
DFRC	KU	80.5 km/h (50 mph)	96.6 km/h (60 mph)	average		DFRC avg.	KU	
I	4	0.455	0.435	0.445	*(0.426) *0.449	-	-	-0.9
	14				(0.436) 0.459	-	-	-3.1
II	16	0.315	0.288	0.302	*(0.270) *0.284	32	37	6.0
III	17	0.314	0.299	0.307	*(0.265) *0.279	31	38	9.1

DFRC = Full-scale tests, Dryden Flight Research Center.

KU = One-tenth scale tests, University of Kansas from reference 5.

( ) = values based on reference area A', as in reference 5.

* - these drag coefficients are for configurations without towing hitch, reference 5 (note, full-scale vehicle had towing hitch).

APPENDICES

APPENDIX A

INTEGRATION PROCESS

$$F = \bar{m}a = -0.5\rho V^2 C_{D_a} A - fW$$

$$f = 0.005 + (0.15/p) + (0.000035\ V^2/p)$$

$$F = \bar{m}a = -0.5\rho V^2 C_{D_a} A - (0.005+(0.15/p)+(0.000035\ V^2/p))W$$

$$a = -(0.5\rho V^2 C_{D_a} A)/\bar{m} - (0.005+(0.15/p)+(0.000035\ V^2/p))(W/\bar{m})$$

$$a = -(0.5\rho V^2 C_{D_a} A)/\bar{m} - 0.000035(V^2 W/p\bar{m}) - (0.005+(0.15/p))(W/\bar{m})$$

$$a = -((0.5\rho C_{D_a} A)/\bar{m} + 0.000035\ W/\bar{m})V^2 - (0.005+(0.15/p))(W/\bar{m})$$

Let $\quad A = ((0.5\rho C_{D_a} A)/\bar{m} + 0.000035\ W/\bar{m})$

$$B = (0.005 + (0.15/p))$$

$$a = \frac{dV}{dt} = -AV^2 - B$$

$$-dt = \frac{dV}{AV^2 + B}$$

Integration Formula

$$\frac{dx}{a + bx^2} = 1/\sqrt{ab}\ \tan^{-1} x\sqrt{ab}/a$$

$$\frac{dV}{AV^2 + B} = 1/\sqrt{BA}\ \tan^{-1} V\sqrt{BA}/B$$

$$-dt = \frac{dV}{B + AV^2}$$

$$-t + to = 1/\sqrt{BA}\ \tan^{-1} V\sqrt{BA}/B - 1/\sqrt{BA}\ \tan^{-1} Vo\sqrt{BA}/B$$

$$-t\sqrt{BA} = \tan^{-1} V\sqrt{BA}/B - \tan^{-1} Vo\sqrt{BA}/B$$

$$\tan^{-1} V\sqrt{BA}/B = \tan^{-1} Vo\sqrt{BA}/B - \sqrt{BA}\ (t)$$

APPENDIX A (continued)

$$V\sqrt{BA}/B = \tan\left(\tan^{-1} Vo\sqrt{BA}/B - \sqrt{BA}\,(t)\right)$$

$$V(t) = (B/\sqrt{BA}) \tan\left(\tan^{-1} Vo\sqrt{BA}/B - \sqrt{BA}\,(t)\right) \qquad \text{Equation 3}$$

Where $A = ((0.5\rho C_{D_a} A)/\bar{m} + 0.000035\ W/\bar{m})$

$B = (0.005 + (0.15/p))$

APPENDIX B

COMPUTER PROGRAM VEHICLE

```
00100     PROGRAM VEHICLE(INPUT,OUTPUT,TAPE5=INPUT,TAPE6=OUTPUT)
00110     EXTERNAL FUNC
00120     INTEGER M,N,IXJAC,NSIG,MAXFN,IOPT,I,INFER,IER
00130     REAL PARM(4),X(2),F(50),XJAC(50,2),XJTJ(1300),WORK(1700),EPS,
00140+    DELTA,SSQ,XJTJ,Y(50),U(50),AD,AF,EM,VO,W,G(50)
00150     COMMON/ZSQ/Y,U,G,AD,EM,AF,VO,W,P,J
00160     L=5
00170     M=1
00180     N=1
00190     NSIG=4
00200     IXJAC=50
00210     EPS=0.0
00220     DELTA=0.0
00230     MAXFN=500
00240     IOPT=1
00250     X(1)=.5
00260     READ(5,*)I,J
00270     READ(5,*)EM,AD,AF,W,VO,P
00280     WRITE(6,50)EM,I,J
00290 50  FORMAT(/,5X,"EFFECTIVE MASS =",F10.4,15X,"RUN  ",I2,"-",I2)
00300     WRITE(6,55)AD
00310 55  FORMAT(/,5X,"AIR DENSITY =",F10.8)
00320     WRITE(6,60)AF
00330 60  FORMAT(/,5X,"FRONTAL AREA =",F10.4)
00340     WRITE(6,65)W
00350 65  FORMAT(/,5X,"WEIGHT =",F10.4)
00360     WRITE(6,70)VO
00370 70  FORMAT(/,5X,"INITIAL VELOCITY =",F10.4)
00380     WRITE(6,73)P
00390 73  FORMAT(/,5X,"EXTRAPOLATED TIRE PRESSURE =",F10.4)
00400     I=1
00410 90  READ(5,*)U(I),Y(I)
00420     J=I
00430     WRITE(6,75)
00440 75  FORMAT(//,8X,"TIME",9X,"VELOCITY")
00450     WRITE(6,80)
00460 80  FORMAT(5X,"****************************",/)
00470     WRITE(6,85)U(I),Y(I)
00480 85  FORMAT(5X,F10.4,5X,F10.4)
00490     CALL ZXSSQ(FUNC,M,N,NSIG,EPS,DELTA,MAXFN,IOPT,PARM,X,SSQ,F,
00500+    XJAC,IXJAC,XJTJ,WORK,INFER,IER)
00510     D=.5*AF*AD*X(1)*(Y(I)**2)
00520     WRITE(6,95)X(1),D
00530 95  FORMAT(//,5X,"COEFFICIENT OF DRAG =",F10.6,5X,"AERO DRAG =",
00540+    F10.6)
```

APPENDIX B (continued)

```
00550     I=I+1
00560     IF(I.LT.L+1) GO TO 90
00570     STOP
00580     END
00590     SUBROUTINE FUNC(X,M,N,F)
00600     INTEGER M,N,I,J
00610     REAL X(N),F(M),Y(50),U(50),G(50)
00620     COMMON/ZSG/Y,U,G,AD,EM,AF,V0,W,P,J
00630     DO 30 I=1,M
00640     T1=(.005+(.15/P))*(W/EM)
00650     T2=SQRT(T1*(((AD*X(1)*AF)/(2*EM))+((.000035*W)/(EM*P))))
00660     G(J)=T1/T2*(TAN(ATAN(T2/T1*V0)-(T2*U(J))))
00670 30  F(I)=Y(J)-G(J)
00680     RETURN
00690     END
```

End of Document